

Article

Atoll Groundwater Movement and Its Response to Climatic and Sea-Level Fluctuations

Ferdinand K. J. Oberle ^{1,*}, Peter W. Swarzenski ² and Curt D. Storlazzi ¹

¹ U.S. Geological Survey, Pacific Coastal and Marine Science Center, Santa Cruz, CA 95060, USA; cstorlazzi@usgs.gov

² International Atomic Energy Agency, 98000 Monaco, Principality of Monaco; p.swarzenski@iaea.org

* Correspondence: foberle@usgs.gov; Tel.: +1-831-460-7589

Academic Editors: Maurizio Polemio and Kristine Walraevens

Received: 26 July 2017; Accepted: 22 August 2017; Published: 30 August 2017

Abstract: Groundwater resources of low-lying atoll islands are threatened due to short-term and long-term changes in rainfall, wave climate, and sea level. A better understanding of how these forcings affect the limited groundwater resources was explored on Roi-Namur in the Republic of the Marshall Islands. As part of a 16-month study, a rarely recorded island-overwash event occurred and the island's aquifer's response was measured. The findings suggest that small-scale overwash events cause an increase in salinity of the freshwater lens that returns to pre-overwash conditions within one month. The overwash event is addressed in the context of climate-related local sea-level change, which suggests that overwash events and associated degradations in freshwater resources are likely to increase in severity in the future due to projected rises in sea level. Other forcings, such as severe rainfall events, were shown to have caused a sudden freshening of the aquifer, with salinity levels returning to pre-rainfall levels within three months. Tidal forcing of the freshwater lens was observed in electrical resistivity profiles, high-resolution conductivity, groundwater-level well measurements and through submarine groundwater discharge calculations. Depth-specific geochemical pore water measurements further assessed and confirmed the distinct boundaries between fresh and saline water masses in the aquifer. The identification of the freshwater lens' saline boundaries is essential for a quantitative evaluation of the aquifers freshwater resources and help understand how these resources may be impacted by climate change and anthropogenic activities.

Keywords: aquifer; atoll; freshwater lens; sea-level rise; flooding; groundwater; tide; submarine groundwater discharge

1. Introduction

In climate change vulnerability assessments, the Marshall Islands as well as the neighboring Kiribati islands, are listed under the “Profound Impacts” category, i.e., the countries “may cease to exist in the event of worst-case scenarios” [1]. A major part of such assessments comes from the limited nature of freshwater resources on low-lying Pacific atoll islands, which is most commonly the critical factor for sustained human habitation. The severity of groundwater dependency was witnessed during a drought in 2016 that caused 16,000 Marshallese, or 30% of the total population to suffer from severe water shortages prompting the Marshallese government to issue a state of emergency [2]. The freshwater resources on low-lying atoll islands typically reside in shallow aquifers, known as freshwater lenses (FWLs), which are naturally recharged only by rainfall and float on top of denser seawater. A brackish transition zone separates saline from fresh water (Figure 1). This hydrogeological setting makes FWLs highly susceptible to vertical mixing that occurs across the entire island and not just at the coastline [3]. In general, the FWL on atoll islands is a function of rainfall, recharge, hydraulic conductivity of the unconsolidated Holocene deposits, and island width, including the reef flat plate

and depth to the Thurber discontinuity [4]. The observed FWLs' thicknesses for atoll islands across the Pacific and Indian Ocean are commonly less than 15 m and rarely exceed 20 m [4].

A number of threats to the FWLs have been identified, including: (a) infiltration of anthropogenic contaminants [5]; (b) upconing of saline water due to excessive freshwater pumping [6]; (c) reduction in reef and island size due to coastal erosion, leading in turn to a reduction in the size of the FWL [7]; (d) droughts that hinder successful recharge of the FWLs [5,8–10]; and (e) storm surges that cause large waves to wash over the atolls resulting in saline intrusion [11–13]. Nonetheless, a better understanding of the processes that influence these FWLs—especially in light of expected climate change scenarios on low-lying atoll islands is essential to better assess atoll water resources management challenges in the near future.

The wide range of temporal variability in hydrological processes on low-lying atoll islands complicates the scientific analysis of these processes, while rendering them all the more important. Against the background of expected rising sea levels and more frequent large wave events, hydrogeologic drivers such as tides and altered rainfall patterns must be better understood as they will affect the freshwater resources and consequently lead to a reduction in habitable and cultivatable land. In order to better understand the future changes to the FWLs of low-lying atoll islands, baseline conditions and their temporal variability have to be clearly defined.

The primary goal of this project was to gain a better understanding of the processes that affect the freshwater lens using high-resolution time-series observations of the marine and hydrologic forcings. The effects of multistressors, such as wave-driven overwash events or large rainfall events, represent one of the least monitored and understood topics within atoll hydrology. Only the coupling of hydrological time-series data with oceanographic time-series data will allow a better prediction of future responses of the FWL to the impacts of climate change. Specifically, we present and discuss both geophysical and geochemical data addressing the forcing of the FWL by tides, rainfall, submarine groundwater discharge, large wave events, and high resolution sea-level rise on Roi-Namur Island on Kwajalein Atoll in the Republic of the Marshall Islands.

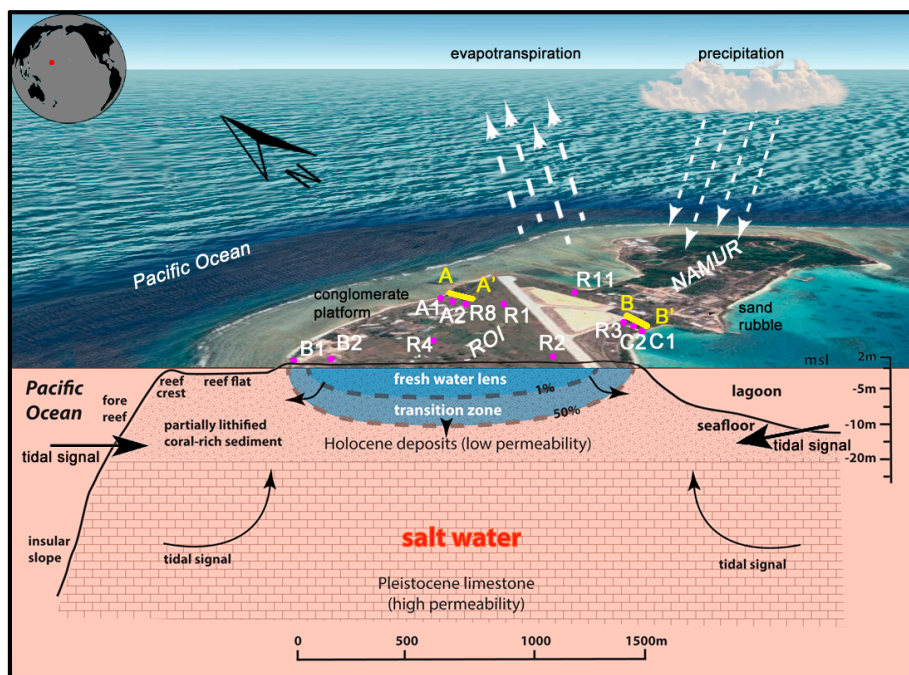


Figure 1. Satellite image and conceptual drawing of the shallow aquifer system of Roi-Namur, Kwajalein Atoll, Marshall Islands. Location of shallow groundwater monitoring wells (magenta dots) and time-series electrical resistivity transects (yellow lines) are indicated.

Study Area

The data presented herein were collected on the island of Roi-Namur (Figure 1) on the northern tip of Kwajalein Atoll in the Republic of the Marshall Islands. Kwajalein is a large (maximum width ~100 km), low-lying (average elevation ~2 m) atoll system with a large, deep (>50 m) lagoon and 97 islets that support variably healthy freshwater lenses [14,15]. In 1944, Roi and Namur Islets, located at the northeast tip of the Kwajalein Atoll (lat. 9°23' N, long. 167°28' E), were connected by the US Navy with artificial fill to form a single island, now measuring 2.5 km². The reef flat is fully exposed (dry) at low tide, is about 250–350-m wide, and covers an area of about 1 km². Most of the groundwater the water supply system utilizes originates from a horizontal, 1000-m long, skimming well lying just below ground surface, parallel to the runway [13]. This type of well-pumping system limits upconing of the deeper saline water during groundwater withdrawals [16].

Previous research shows the shallow aquifer system at Roi-Namur Island is composed of unconsolidated, reef-derived, calcium-carbonate sand and gravel, with few layers of consolidated rock (coral, sandstone, and conglomerate). The island consists of an approximately 2-m thick disturbed surface layer underlain by three Holocene layers, with a combined thickness of approximately 20 m (Figure 1). This overlays a highly permeable Pleistocene deposit in the order of 900 m thick [14,17]. Aquifer horizontal permeability (*k*) has previously been calculated to be 1×10^{-11} – 2×10^{-10} m² (hydraulic conductivity [*K*]: 1×10^{-4} – 1.6×10^{-3} m/s) in the upper Holocene layers and about 3.5×10^{-10} m² (*K*: 3.2×10^{-3} m/s) in the lower Pleistocene layer [17]. Roi-Namur's FWL thickness has been shown to vary according to levels of recharge, ranging from 5–12 m thick [13,16]. The groundwater on Roi-Namur is artificially recharged using stored rainwater; this artificial recharge amounts to approximately 3.5% of the natural recharge from rain (66×10^6 L/year for the years 2000–2012) and started in 2009 [13]. The available potable freshwater supply has been estimated to 86×10^7 L for Roi and 16×10^6 L for Namur [16]. A more general overview on the effects of groundwater pumping on the FWL can be found in Terry et al. [18].

Previous studies [19,20] have demonstrated that global sea level is rising at a rate almost double the Intergovernmental Panel on Climate Change's (IPCC) 2007 report in this area. These high rates of sea-level rise have been tied to strengthened easterly trade winds, which, in turn, appear to be driven by variations in the latent heat content of the earth's warming atmosphere, suggesting that this trend is likely to continue under projected emission scenarios e.g., [21]. Furthermore, the projected sea-level rise will outstrip potential new reef flat accretion, for optimal vertical coral reef flat accretion rates for coral reefs exposed to open-ocean storm waves are up to an order of magnitude smaller (1–4 mm/year per [22,23] than the rates of sea-level rise projected for the years 2000–2100 (8–16 mm/year per [24,25]). For Roi-Namur, this projected scenario results in a net increase in water depth over exposed coral reef flats at the order of 0.4–1.5 m during the 21st century, which will result in larger wave heights [26] and an increase of up to 200% in wave run-up [27], and may ultimately lead to a complete drowning of the islets [28].

2. Materials and Methods

2.1. Groundwater Levels, Temperature, Specific Conductivity (Salinity) and Water Geochemistry

An assessment of Roi-Namur's shallow freshwater lens was carried out from November 2013 to April 2015. This assessment included surveys of groundwater levels, temperature and specific conductivity (salinity) in a suite of temporary, shallow monitoring wells strategically placed around the island (Figure 1). The wells were constructed of 4-cm-diameter polyvinyl chloride (PVC) pipe with a 60-cm screened section set 15 cm above the bottom to allow groundwater to flow into the well only from the desired depths. Time-series groundwater levels and specific conductivity measurements were performed every 15 min using factory-calibrated Solinst LTC Leveloggers, while time-series groundwater temperature measurements were obtained every 20 min using factory calibrated Onset HOBO temperature loggers. Additionally, depth-specific groundwater samples were collected with an

AMS Piezometer Groundwater Sampling Kit alongside a calibrated YSI 556 multiprobe meter between wells C1 and C2 (Figure 1) using protocols of the USGS National Field Manual [29]. The groundwater samples, that were pumped from a depth of up to 8 m, were analyzed for ammonium (NH^+4), dissolved silicate (DSi), total dissolved phosphorus (TDP), molybdenum (Mo), barium (Ba), uranium (U), and a suite of hydrological parameters, including pH and salinity. As per methods summarized in Swarzenski et al. [30] nutrients were determined on a Lachat Instruments QuickChem 8000 at Woods Hole Oceanographic Institute (WHOI), while the suite of trace elements was analyzed on a High Resolution Inductively Coupled Plasma Mass Spectrometer at the University of Southern Mississippi. From these measurements, tidal lag and efficiency could also be determined, and is useful for estimating aquifer permeability and storage properties [15].

2.2. Electrical Resistivity Tomography (ERT) Surveys

The utility of electrical resistivity to examine the dynamics and scales of the freshwater/saltwater interface in coastal groundwater is well established [31–33]. Time-series multichannel, electrical resistivity tomography (ERT) surveys were conducted along two transects (A–A' and B–B' on Figure 1) during both high and low tides in March 2013. Because the survey cable remained fixed in position on the ground surface during the high tide/low tide and no acquisition parameters were altered during collection, the observed changes in resistivity are only a function of the tidally-modulated pore–fluid exchange. Transects were aligned perpendicularly to the shoreline and located 0.75 m above mean sea level. A SuperSting R8 system (Advanced Geosciences Inc. [AGI], Austin, TX, USA) was used to measure the electrical resistivity of the subsurface along a 56-electrode cable (consistently spaced either 1- or 2-m apart). Each electrode was pinned to the underlying sediment with a 35-cm stainless steel spike. The electrical resistivity measurements were acquired using a dipole-dipole array setting. The relative elevation of each electrode was carefully measured using a Theodelite and the topographic change incorporated into inverse modeling routines (AGI EarthImager).

2.3. Submarine Groundwater Discharge (SGD)

Coastal submarine groundwater discharge (SGD) is a highly dynamic and complex hydrogeological phenomenon that involves both terrestrial and marine drivers that define the amount and rate of submarine discharge into the coastal sea, which also incorporates the exchange of water masses through seawater intrusion into the aquifer [34]. Quantification of SGD rates, even in groundwater limited atoll settings, is important to assess groundwater exchange mechanisms and associated constituent fluxes across the island shoreface. The utility of ^{222}Rn as a water mass tracer is well-proven to study rates of SGD due to its very short half-life (3.8 d) and its multifold enrichment in groundwater relative to surface water [35]. RAD7 radon detection systems were employed to measure Rn in air using a water/air exchanger. This setup allows for a near real-time calculation of the aqueous Rn concentration by measuring the air ^{222}Rn concentration and knowing the temperature-dependent ^{222}Rn partitioning coefficient [31,36–40]. A peristaltic pump was used to produce a continuous stream of coastal surface water into the water/air exchanger, while air from the exchanger was continuously pumped into the RAD7 radon monitor. The RAD7 contains a solid-state, planar, Si alpha (PIPS) detector and converts alpha radiation into usable electronic signals that can discriminate various short-lived daughter products (e.g., ^{218}Po , ^{214}Po) from ^{222}Rn [41]. Time-series measurements of nearshore seawater ^{222}Rn were obtained using a single RAD7 radon monitor setup for 30-min counting intervals. An additional onsite monitoring station was set up at well R3 (Figure 1) to establish a ^{222}Rn groundwater endmember. ^{222}Rn time-series measurements were taken every 30 minutes for 12 h. The ^{222}Rn endmember value was established after measurements at peak values had fully leveled ($n = 10$). For the ^{222}Rn time-series, the surface- and bottom-waters were instrumented with Solinst LTC Leveloggers that continuously measured pressure, conductivity, and temperature of ambient seawater. A simple non-steady state radon mass-balance box model was then employed for calculations of SGD following methods developed by Burnett and Dulaiova [36] and Burnett et al. [35]. In general, this box

model accounts for radon sources from (a) total benthic fluxes via submarine groundwater discharge (SGD); (b) diffusion from sediments; and (c) production from dissolved ^{226}Ra . Radon losses were calculated by including gas evasion, radioactive decay, and mixing with offshore radon-depleted water. In all cases, the excess inventory per time (i.e., differences between source and sink fluxes) was divided by radon concentration in groundwater (i.e., groundwater endmember) to calculate groundwater discharge. Site locations for these surface water time-series deployments were strategically placed based on previous data e.g., [13,16,42], and assumptions on gradients in oceanographic, geologic, and hydrologic controls (Figure 1).

3. Results

The ERT profiles clearly identified the FWL in the nearshore environment by recording salinization with depth, as confirmed with deep pore-water sampling (Figure 2). Although the horizontal variability in the ERT profiles may be interpreted as freshwater fingers related to tidally induced convective forcing as has been shown to occur in models [43,44], it is more likely that it is influenced by near-surface variations in conductivity of the soil matrix. However, the overall homogeneity of the aquifer’s substrate was found to be relatively uniform as observed by measurements of the hydraulic pressure signal that propagates from the island perimeter inward through the geologic framework of the island.

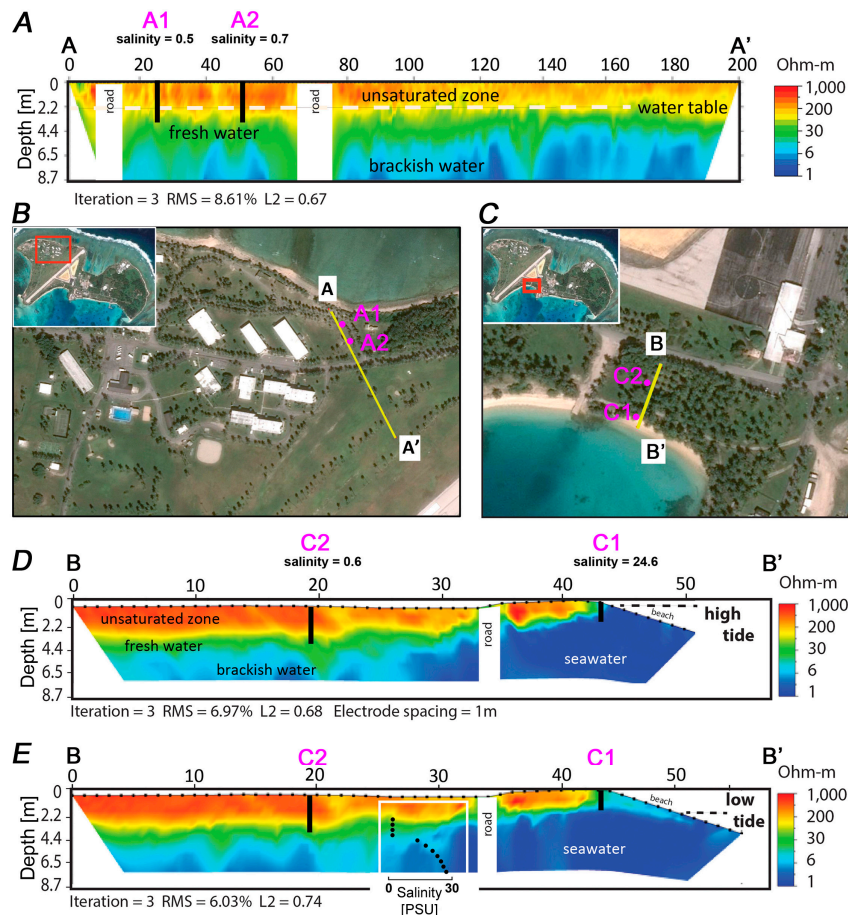


Figure 2. Locations and examples of Electrical Resistivity Tomography (ERT) profiles; (A) ERT profile A–A’ on the ocean side of Roi; (B) Map showing location of ERT profile A–A’; (C). Map showing location of ERT profile B–B’; (D). ERT profile B–B’ on the lagoon side of Roi at high tide; (E). ERT profile B–B’ on the lagoon side of Roi at low tide. The locations of wells A1, A2, C1, and C2 are denoted in magenta. The pore water salinity profile shown in the lower image was obtained using a drive point piezometer, as described in Section 3.1.

Although the ERT profiles clearly identified a distinct FWL floating atop seawater (Figure 2), they were also ground-truthed through geochemical pore water profiles (Figure 3) along the same lagoonal transect (B-B', Figure 2). Most geochemical analyses recorded a sharp transition zone below 4 m depth, indicating a zone of mixing and a differentiation of unique water masses. Salinities sharply increased below 4 m from a freshwater environment (salinity = 1) to a saline environment (salinity = 28). Approximately fourfold similar increases between the water masses were measured in ammonium (NH_4^+), phosphate (PO_4^{3-}), molybdenum (Mo), uranium (U), and pH. On the other hand, barium (Ba) and silicate (Si) were highest near the surface and decreased with depth at more gradual rates.

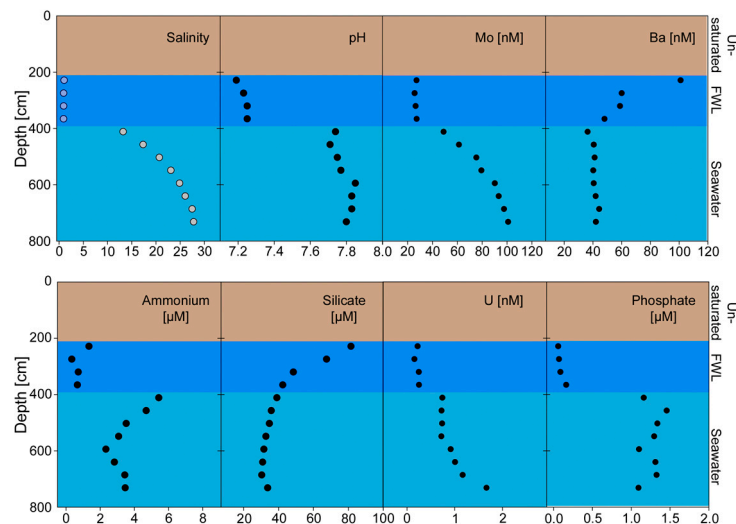


Figure 3. Geochemical pore water profiles demonstrating the sharp transition zone between the FWL and the underlying saline groundwater. Site location for these pore water profiles is indicated on Figure 2 between wells C1 and C2.

In order to evaluate the islands permeability and poroelastic storage capacity, a measurement of the attenuation of the tidal signal was captured as tidal efficiency and tidal lag. Tidal efficiency is the amplitude ratio between the magnitudes of the response seen in a well and the corresponding tides. Tidal lag is the time difference or phase lag between the tidal peak and the aquifer response peak. In general, this pressure signal is dampened by frictional losses related to the permeability and the poroelastic storage capacity of the aquifer. Consequently, it is important to assess tidal lag and efficiency in order to address the homogeneity of the aquifer's substrate. Tidal efficiencies from the shallow monitoring wells ranged from 7 to 63%, while the tidal lag ranged from 40 to 170 min for wells measured at 3 m of groundwater depth relative to mean sea level. The measurements of tidal lag and efficiency attained from multiple coastal wells at 3-m depth fit well ($R^2 = 0.9$) with the previously published data by Gingerich [42] (in Peterson [45]) and demonstrate that tidal attenuation is predictably dependent on the distance from the shoreline (Figure 4). Gingerich [42] demonstrated that tidal lag and efficiency were also dependent on the depth of each well, showing that deeper wells had higher efficiencies as the signal traveled through the Pleistocene layer and then upward through the Holocene layer.

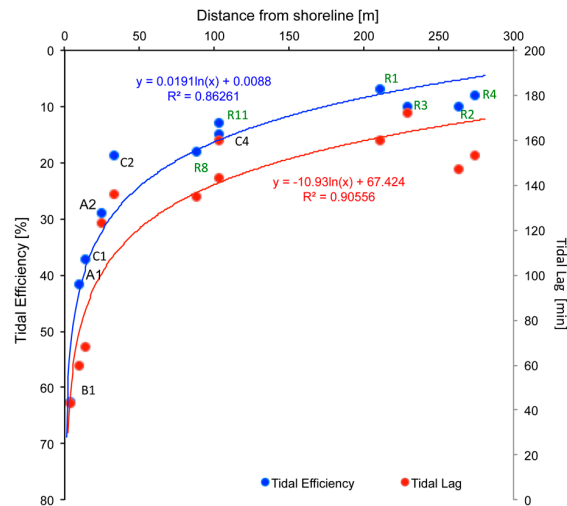


Figure 4. Tidal efficiency and tidal lag calculations for groundwater wells. Groundwater well locations shown in Figure 1. Data for groundwater wells R1–R11 (green) were published by Gingerich, 1992 and normalized to 3 m depth using a linear relationship.

3.1. Tidal Effect

The dominant driver for the repetitive changes in salinity and groundwater level on Roi-Namur is the oceanic tide (Figure 5A). The measurements show that conductivity can vary up to 10,000 $\mu\text{S}/\text{cm}$ within a single tidal cycle (Figure 5B). These changes in conductivity, as a proxy for salinity, are also synchronized with changes in groundwater levels, both temporally and in magnitude. Consequently, spring tides cause the greatest rise of groundwater levels (maximum = 0.75 m) and salinity (maximum conductivity = 10,000 $\mu\text{S}/\text{cm}$), while neap tides are expressed as having a significantly lower groundwater levels (maximum = 0.20 m) and salinities (maximum conductivity = 2000 $\mu\text{S}/\text{cm}$). The ERT profiles also imaged the vertical shift of the FWL with the tidal oscillations. Groundwater wells within the ERT profiles confirmed this by recording freshwater during low tides and in seawater during high tides at their base (Figure 2D,E).

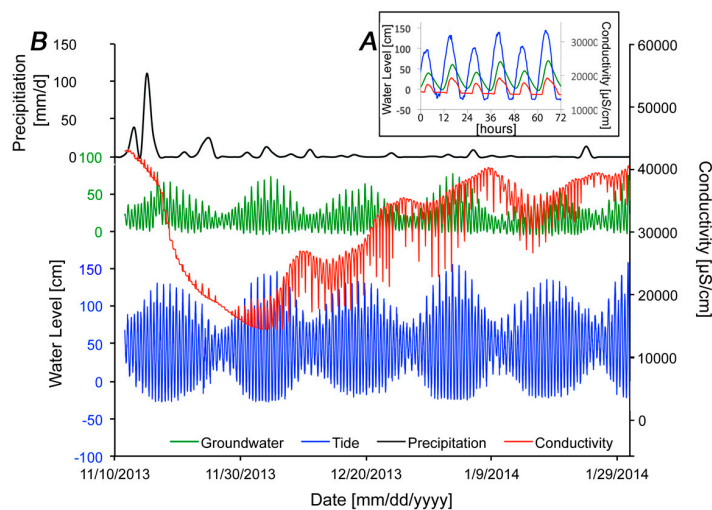


Figure 5. Time series plots showing tidal forcing of groundwater levels and salinity (Well C1), as well as the observed response to a large rain event. (A) From 11 November 2013 through 29 January 2014. (B) From 1 December through 4 December 2013. Precipitation gauge data available from NASA/RTS (2017) [46].

On the same tidally controlled temporal scale, SGD also fluctuated between high and low tide (Figure 6). Although SGD rates were generally quite low (average ~1 cm/d), SGD rates varied between 0–3 cm/d. Increased SGD rates were observed shortly after low tide, whereas high tides caused a landward seawater hydraulic head gradient that limited SGD. The ERT profiles confirm this aquifer dynamic (Figure 2D,E), displaying no obvious SGD during high tide but increased brackish discharge during low tide.

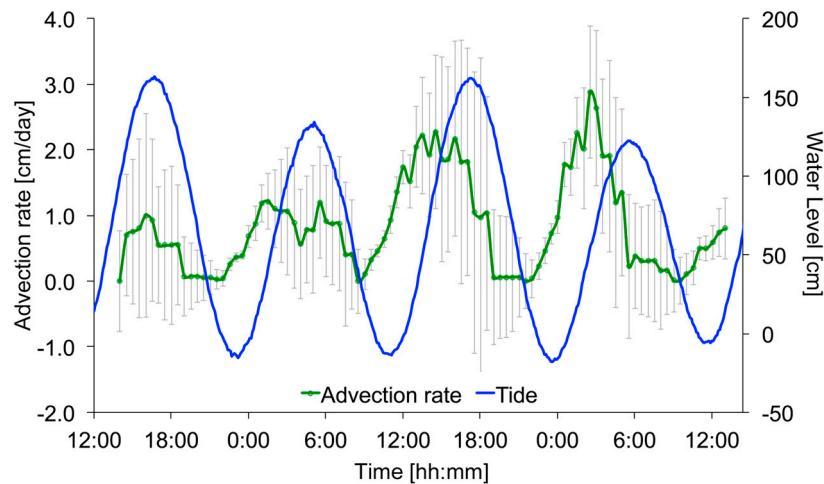


Figure 6. Time series showing ocean water levels (tides, in blue) and the computed submarine groundwater discharge (SGD, in green) advection rates. The error bars denote ± 1 standard deviation.

3.2. Rainfall Effect

The size of the FWLs of low-lying atolls such as Roi-Namur is largely dependent on the rainfall recharge rate and its temporal variation, such as seasonal and interannual rainfall variability related to the El Niño-Southern Oscillation (ENSO) [8,10] plus groundwater extractions [3,13]. In general however, the rate at which the FWL responds to a large rainfall event depends on the duration and intensity of rainfall. The time-series data captured a large scale rain event (Figure 5B) lasting five days, during which approximately 10% of the annual rainfall (~160–190 cm/year) occurred [13,42]. Such rainfall events are often tied to large low pressure systems and are not uncommon on Roi-Namur [47]. The response to this rain event was recorded in the monitoring wells by a relatively rapid freshening of the aquifer, followed by a gradual increase in conductivity (Figure 5B). The initial decrease in conductivity by 64% (or 25,000 $\mu\text{S}/\text{cm}$) caused by this rain event occurred over a 30-d period, while the return to salinity levels prior to the rain event took approximately 3 mo with little rain (8 cm) falling during this period. The groundwater level observed in the wells was only elevated 25 cm for 24 h directly after the large rainfall. This indicates that increased rates in SGD due to rainfall occurred only for a short time period following the rain event, but were not correlative with the associated decreases or increases in salinity.

3.3. Large Wave and Overwash Effect

On 2–3 March 2014, a series of large waves struck Roi-Namur, resulting in wave-driven flooding of the northern portion of the island. The oceanographic forcing that led to this event has been documented in detail by Quataert et al. [27] and Cheriton et al. [48]. The large wave event, which had almost 7-m high waves with 15-s periods, coincided with a spring high tide and caused ocean water surface elevations, combined with wave run-up, to be 3.7 m above the reef flat, resulting in minor seawater flooding of select low-lying inland areas (Figure 7).



Figure 7. Photos of wave-driven flooding and overwash on Roi-Namur Atoll, Republic of the Marshall Islands near the north end of the runway. Photo on the left is looking west and photo on the right is looking east. Red dot on subplot (left photo) indicates the photos location on Roi-Namur.

The event was evidenced in groundwater wells A1, A2, B1, B2, C1, C2, and R3 where it caused an increase in salinity levels e.g., (Figure 8). The overwash event was also accompanied by a sudden and significant rise in groundwater level (20% over the tidally attributed effect) in all wells. The overwash's effect on salinities in wells A1, A2, B1, B2, C1, C2 and R3 was likely dampened by two large rain events that occurred 10 d prior and 1 d (Figure 9) after the overwash event, causing a more gradual signal of increasing salinity than is typical e.g., [9] of saline intrusion. The salinity levels at the nearshore well location A1 closest to the areas flooded with seawater returned to pre-overwash levels within 1 month (Figure 8). Groundwater wells on the lagoonal side of the island returned to pre-overwash salinity levels within 3 d after the overwash event (Figure 9).

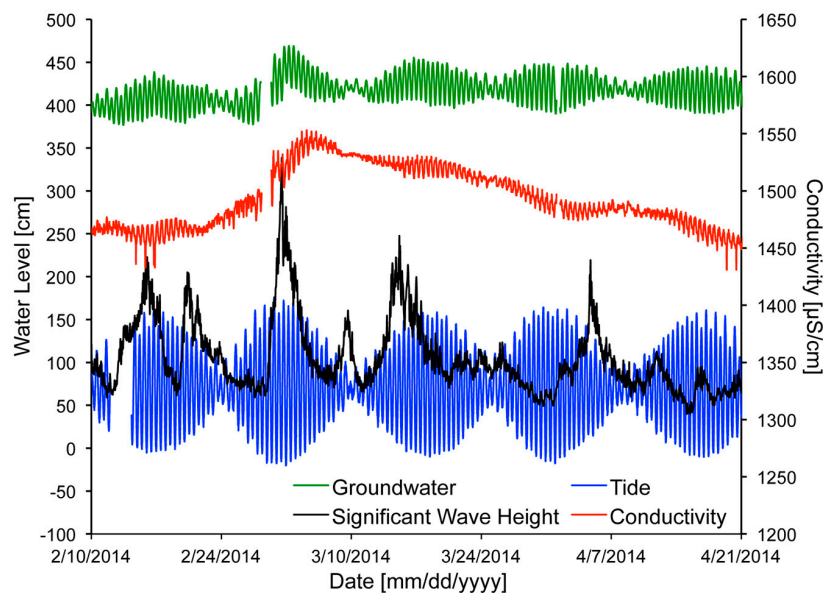


Figure 8. Observed variations in conductivity and ground water level in well A1 following an island overwash event driven by increased significant wave height during 2–3 March 2014.

3.4. Long-Term Rainfall Effect

With the exception of the two large rain events during November 2013 and March 2014, the collected data support the known rainfall patterns: a relatively dry season from December to April, followed by a wetter season with maximum rainfall occurring between August and October (Figure 9).

During the study period from November 2013 through February 2015, rainfall on Roi-Namur amounted to a total of 274 cm, or 198 cm/year. A substantial portion of the total rainfall occurred in the form of two significant storm events followed by periods of significantly reduced rainfall. The large rain event of November 2013 marked the beginning of what was later to become Typhoon Haiyan near the Philippines, one of the most intense and destructive tropical cyclones on record [49]. The annual fluctuation of salinity in groundwater wells was directly correlative to the annual rainfall patterns, as well as the large storm-induced rainfall events in November 2013 and March 2014 that caused a rapid reduction in conductivity. The three largest rainfall events within the study period occurred on 15 November 2013, 21 February 2014 and 6 September 2014, and were all followed by record minimum salinity levels 30–35 days afterwards. The likelihood of this correlation occurring randomly is less than 1% for the data sets of this study period. In the inland well R3, where oceanographic signals interfere less, a reduction in conductivity of 1000 $\mu\text{S}/\text{cm}$ was recorded (Figure 9) after these rainfall events. Although these storm events also caused a sudden increase in groundwater levels, these increases were short-lived (maximum duration of 2 d) and long-term rainfall trends could not be linked to groundwater levels, which steadily decreased over the duration of the study.

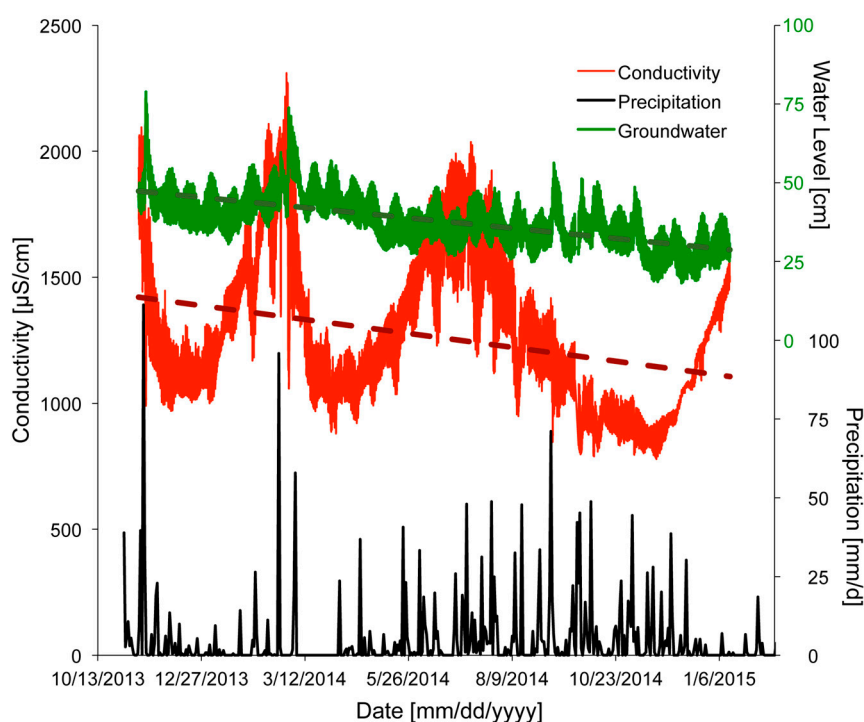


Figure 9. Time series plot showing variations in rainfall (black), groundwater level (green), and conductivity of water (red) in well R3 observed between November 2013 and February 2015. Linear fits to the data are denoted by dotted lines.

3.5. Sea-Level Change Effect

By comparison to the beginning of the 16-mo monitoring period, the observed salinity and groundwater levels fell by approximately 29% and 68%, respectively (Figure 9). Although a water table is never truly stable, the observed negative trend in groundwater height is closely correlative to the varying levels of decline in mean sea level (average 59%) during this time period (Figure 10A). While mean sea level (MSL) measured by tide gauges since 1948 has, on average, been rising at Roi-Namur by 2.2 mm/year (Figure 10B), previous studies [50,51] have shown that during a significant El Niño-Southern Oscillation (ENSO) event a reduction in local mean sea level can occur. Because the monitoring period of this study fell into a time frame of a strong ENSO event, a decrease in MSL of 13.56 cm total or 11.56 cm/year was observed. Discrepancies between groundwater levels and the fall

of MSL were most pronounced during January–March 2014 in Well R11 (Figure 10A). In conjunction with a large decrease in salinity during this time frame (Figure 10A), this discrepancy may indicate the presence of artificial recharge of the FWL as described by Gingerich et al. [13] that would yield higher groundwater levels than from natural sea-level forcing alone. For the study period after March 2014, a cross-correlation analysis of the MSL and the groundwater level data revealed a maximum correlation of 76% at a 5-h shift. However, a definitive answer to this question requires a more detailed analysis of artificial recharge volume, location, and timing.

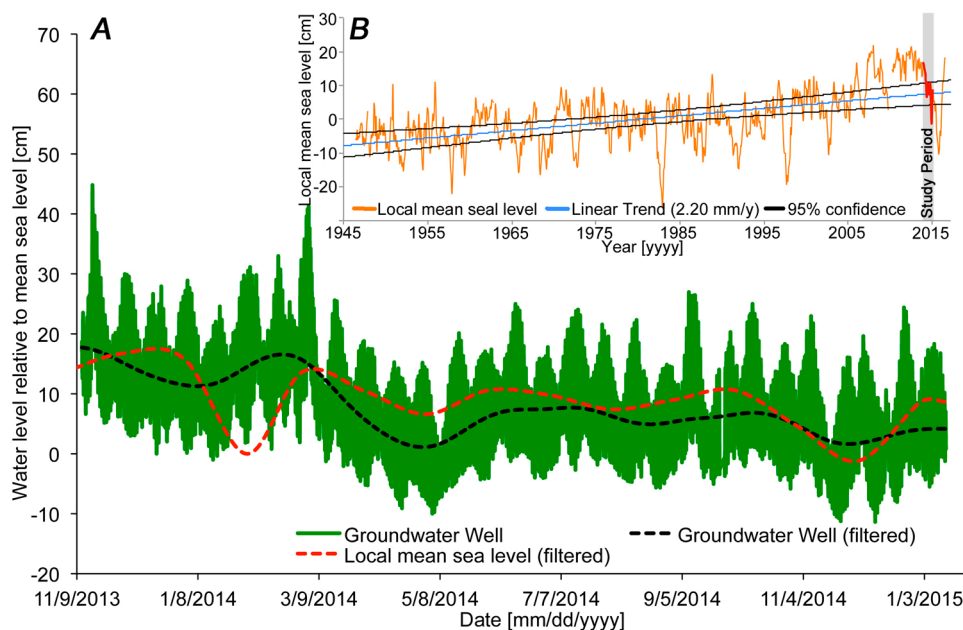


Figure 10. Time series of sea-level forcing and well response; (A) Comparison of groundwater levels and sea levels during the study at Well R11; (B) Local mean sea-level curve from 1945 to 2017. Period pertaining to this study is marked in gray. Sea level data for Kwajalein Atoll from NOAA [52]. A Butterworth filter with a frequency cutoff of 60 d was used to filter data.

4. Discussion

High-resolution temporal observations and analyses of hydrological and oceanographic processes are essential for responsible water resources management on atoll islands, and are especially valuable for natural hazard risk reduction. For Roi-Namur, the results of this study indicate that multiple stressors variably affect the freshwater resources. Whereas the size of the FWL is a function of (1) the geological framework and (2) the hydrodynamics of a two-fluid miscible groundwater system e.g., [1], the temporal variability of the atmospheric (rainfall) and oceanographic (tide, wave and sea-level) forcing play a dominant role for both groundwater levels and hydrogeochemistry.

The influence of sea level caused by spring tides forced the greatest range of variability of groundwater levels and conductivity (salinity) levels, whereas neap tides drive significantly lower variability in groundwater level and conductivity (salinity) levels. The hourly changes in groundwater levels and conductivity (salinity) levels caused by the semidiurnal tidal pressure wave were also the most apparent groundwater signal in all collected datasets e.g., (Figures 5, 6 and 8). This dynamic is expected to be a common response on low-lying carbonate atoll islands and confirms previous studies on tide-induced fluctuations of salinity and groundwater level in unconfined aquifers [53].

The tidal measurements represent a vertically and horizontally averaged response of the aquifer to a pressure wave passing through an unknown section of the aquifer to reach the well. Gingerich [42] previously showed that tidal efficiency is a function of the dual aquifer effect of the more permeable Pleistocene limestone topped by lesser permeable Holocene deposits (Figure 1). Although those results

focused on the propagation of the tide with increasing aquifer depth, the results presented here, which were normalized to a common depth of 3 m, show that the tidal lag and efficiency are also strongly dependent on the distance to shoreline (Figure 4). Although this may appear obvious, the significant logarithmic fit ($R^2 = 90$) of the tidal lag and efficiency to shoreline distance implies a relatively high homogeneity of the poroelastic aquifer's composition.

Detailed analyses of sea level forces are specifically important in environments with expected low SGD because tidal oscillation may considerably increase the average recirculated seawater component of coastal groundwater [54]. The relatively low SGD rates for Roi-Namur (mean = 1 ± 3 cm/d) fit with previously published SGD rates from low-lying atoll islands with similar atmospheric and oceanographic forcing [55]. For the southern Pacific Rarotonga Atoll, which is considerably higher but experiences similar levels of rainfall (190 cm) and oceanographic forcing, recent SGD calculations suggest similar flow rates of 0.2–1.8 cm/d [56]. The variable SGD flow rates between high tide and low tide are known as tidal pumping, and are the main driving force of pore water advection. SGD-induced tidal pumping has previously been described as the “breathing” of offshore coral islands, where seawater is inhaled at high tide and nutrient rich groundwater is exhaled at low tide, leading to sustained productivity within coral reefs [57].

Furthermore, the analysis of tidally driven SGD is also important for a more complete understanding of aquifer biogeochemistry and reef health. SGD has been shown to play a major ecological factor connecting the reef to the subsurface environment, which, may in turn lead to connections to land e.g., [41,58,59]. The geochemical loading from SGD has been described as comparable to or exceeding those of surface runoff inputs, due to higher dissolved solids concentrations in groundwater and larger accumulative discharge zones [41,60]. Contrary to these findings, nutrient levels such as phosphate or ammonium from freshwater SGD on Roi-Namur are roughly four times lower than the seawater underlying the island (Figure 3). The increasing levels of ammonium with depth is likely caused by dissimilatory nitrate reduction that occurs in the more anoxic conditions in the deeper parts of the aquifer [61]. The phosphate enrichment in the deeper saline waters have previously been associated with carbonate dissolution. Burt [62] showed that saltwater penetrating a carbonate aquifer is enriched with ammonia and phosphate, relative to fresh groundwater end-members. He attributed these enrichments to calcite dissolution processes of the carbonate aquifer structure driven by CO_2 infiltration. On Roi-Namur, Hejazian et al. [16] have shown that the carbonate dissolution leads to increased porosity of the aquifer and a downward transport of undersaturated waters. Similar sharp increases with depth in Mo, U, and pH are likely reflective of an oxygenated freshwater environment (<4 m depth) and a more anoxic saline environment (>4 m depth). While the geochemical data clearly suggest a separation of the FWL from the underlying seawater at 4 m depth, some minor freshwater mixing that decreases with depth is indicated within the more anoxic saline environment (>4 m depth) by salinity, Mo or Si levels. The high surficial levels in Ba and Si imply a surficial anthropogenic source, such as the building materials used in the construction of the runway on Roi-Namur. This would also explain their gradual reduction with depth. In general, this indicates that freshwater SGD is not likely to cause a significant nutrient input to nearshore waters, whereas the tidal flushing of deeper saline groundwater may contribute to nutrients to the reef.

Contrary to the rhythmic, predictable hydrological processes driven by tidal oscillations, storm events and their associated hydrological drivers, such as rainfall and wave-driven flooding, occur less predictably. The high temporal variability of rainfall on Roi-Namur observed during this study confirmed previous analysis of a relatively dry season from December to April, followed by a wetter season with maximum rainfall occurring between August and October. This study shows that heavy rainfall events, such as those caused by storm systems, can significantly and suddenly alter the conductivity (salinity) levels in groundwater wells (Figure 5), while periods of drought or reduced rainfall cause a gradual increase in groundwater wells' salinities (Figure 9). On Roi-Namur and elsewhere in Marshall Islands, this can become particularly important, as rainfall can decrease by 80% during El Niño droughts [63], causing more than half of the Marshall Islands to be classified as

“highly vulnerable” to freshwater stress [10]. Model calculations have also shown that during drought, groundwater on small islands (<300 m width) can be completely depleted [10]. In addition, the most recent predictions by the Department of Defense’s Strategic Environmental Research and Development Program [64] forecast significant decreases in rainfall. The latter prediction is also supported by measured rainfall data since 1950 that shows a decreasing trend in annual and seasonal rainfall [65]. Nonetheless, there still exists uncertainty around the rainfall projections and not all models show consistent results [47].

Although Roi-Namur lies within a climatic zone where rainfall and storms are likely to occur during specific times of the year, their exact temporal occurrence, specifically in relation to regional sea level and tidal oscillations, is harder to predict. Consequently, concurrent high wave events and spring tides leading to island overwash and seawater flooding occur with little warning [48]. Although the overwash event recorded in this study caused conductivity (salinity) increases that recovered after approximately one month (Figure 8) in affected groundwater wells, more severe overwash events have the potential to be catastrophic, leading to FWL recovery times of 22–26 months [11–13]. For example, in 2008, 2009, and 2011, storm-driven large wave events that coincided with high tides negatively affected freshwater drinking supplies, destroyed vital crops, demolished infrastructure, and killed hundreds of thousands of Federally-protected animal species on Pacific atolls [12,66], highlighting the exceptional vulnerability of these low-lying island communities. We suggest that future work should focus on further developing wave run-up forecasting tools for Roi-Namur and other Pacific Islands [67] and integrating quantitative saline intrusion predictions, thereby not only protecting buildings and general infrastructure, but also the islands’ vital freshwater resources.

The recorded conductivity data indicate that the overarching control on salinity levels detected in groundwater wells is not driven by rainfall alone, but a combination of changes in rainfall and sea level. Although tidal pressure causes oscillations in wells’ conductivity (salinity) profiles, the longer-term control on salinity levels in groundwater wells can be attributed to a local change in MSL. This can be observed in the slope of the recorded conductivity data that is congruent with the average decline in MSL over the course of this study (Figure 9). The observed dependence of groundwater conductivity levels on MSL indicates that salinity levels in groundwater wells should also increase in the future in accordance with the predicted future rise in MSL.

Mean sea level is projected to continue to rise over the course of the 21st century and there is very high confidence in the direction of change [68]. The most current models simulate a rise in mean sea level between 7 and 19 cm by 2030 using the full range of emission scenarios. Increases in mean sea level of 41–92 cm by 2090 under the Representative Concentration Pathways emission scenario, 8.5 can be expected [69]. The predicted rise in eustatic sea level will also increase the size of large waves over coral reefs and the resulting wave-driven run-up, leading to more frequent and intense overwash events in the future [26]. Although the documented overwash event in this study occurred over a relatively short timeframe (3 h) when the spring tide and the high wave event overlapped, the predicted future sea-level rise will allow overwash events to occur during a much longer portion of the tidal cycle. This also means that in the future, as sea-level rise continues, smaller wave events, which also occur more frequently, will be able to cause island flooding and negatively impact the island’s freshwater resources.

5. Conclusions

FWLs on small low-lying atoll islands such as Roi-Namur are under constant and ever-increasing threat of salinization. Yet, it is these groundwater resources that are critical for the survival of the local population. The potential threats to the salinity levels of the FWLs are abundant and occur in the form of high tides—especially king tides, lack of rainfall, large wave events, and sea-level rise. Other anthropogenic threats not considered in this study include contamination, over-extraction, and island modification.

This study provides measured responses of conductivity (salinity) in groundwater wells to severe rainfall events, as well as seasonal rainfall patterns. The study provides calculations on tidal lag and efficiency in wells normalized to 3-m depth that demonstrate tidal attenuation is predictably dependent on the distance from the shoreline. An island overwash event was documented and the nearshore aquifer responses identified. ERT profiles characterized the freshwater outflow patterns and the FWL's saline boundaries. Depth-specific geochemical pore water measurements characterized and confirm the distinct boundaries between fresh and saline water masses in the aquifer. SGD was calculated and put in the context of tidal oscillations to show its varying degrees of output. Conductivity (salinity) and groundwater levels were shown to respond to measured mean local sea-level change.

The results show that the impact of the individual threats on the FWLs is strongly dependent on their relative timing. As expected, spring tides were observed to cause the greatest rise of groundwater levels and conductivity (salinity), whereas neap tides are expressed as having a significantly lower groundwater levels and salinities. Tidal oscillations could be identified in both groundwater levels and conductivity (salinity) levels. The tidal signal was also expressed in SGD, which ceased to exist during high tides, effectively allowing saline waters to intrude the outer limits of the FWL, while low tides allowed freshwater to be expelled into the lagoon. Tidal lag and efficiency were reflective of a highly permeable substrate that was homogenous throughout the of the island's nearshore surficial aquifer strata. Large rain events were shown to have a relatively sudden freshening effect in groundwater wells (within 3 d), while returns to initial conductivity (salinity) levels took up to an order of magnitude longer (30 d). The observed overwash event caused short-lived increases in groundwater levels and an increase in conductivity (salinity) levels that recovered after 1 mo; this event was minor by comparison to previous events that had recovery times of up to 26 mo. Groundwater levels and salinity levels were observed to follow the general falling trend in MSL caused by an El Niño-Southern Oscillation event during this study. Together, these observations demonstrate the atoll aquifer's response to a wide range of atmospheric and oceanographic forcing over a range of temporal scales, and provides insight into the vulnerability of the FWL that will likely heighten with the predicted changes in rainfall and sea level due to global climate change.

Acknowledgments: Funding for this research was provided by the U.S. Department of Defense's Strategic Environmental Research and Development Program (SERDP) under Project RC-2334 and the U.S. Geological Survey's Coastal and Marine Geology Program. The IAEA is grateful for the support provided to its Environment Laboratories by the Government of the Principality of Monaco. We thank S.B. Gingerich for his foresight in developing a groundwater monitoring network on Roi-Namur. We also thank C. Johnson and K.O. Odigie for their help with instrument deployment and data collection. We also thank the Captain and crew of the D/V Patriot, D. Miller and C. Nakasone (Kwajalein Range Services), and the U.S. Army Garrison-Kwajalein Atoll (USAG-KA) for their support of this project. Any use of trade, firm, or product names is for descriptive purposes only and does not imply endorsement by the U.S. Government.

Author Contributions: F.K.J.O., P.W.S. and C.D.S. conceived and designed the experiments; F.K.J.O. and P.W.S. and C.D.S. performed the experiments; F.K.J.O. and P.W.S. analyzed the data; F.K.J.O., P.W.S. and C.D.S. wrote the paper. Authorship must be limited to those who have contributed substantially to the work reported.

Conflicts of Interest: The authors declare no conflicts of interest. The founding sponsors had no role in the design of the study; in the collection, analyses, or interpretation of data; in the writing of the manuscript, and in the decision to publish the results.

References

1. Pernetta, J.C. Impacts of climate change and sea-level rise on small island states. *Glob. Environ. Chang.* **1992**, *2*, 19–31. [[CrossRef](#)]
2. Government of the Marshall Islands. Immediate Drought Response Plan For the Republic of the Marshall Islands Complementing the Declaration on State of Emergency. Available online: <http://reliefweb.int/report/marshall-islands/immediate-drought-response-plan-republic-marshall-islands> (accessed on 26 August 2017).
3. Underwood, M.R.; Peterson, F.L.; Voss, C.I. Groundwater lens dynamics of Atoll Islands. *Water Resour. Res.* **1992**, *28*, 2889–2902. [[CrossRef](#)]

4. Bailey, R.T.; Jenson, J.W.; Olsen, A.E. Estimating the Ground Water Resources of Atoll Islands. *Water* **2010**, *2*, 1–27. [[CrossRef](#)]
5. White, I.; Falkland, T.; Perez, P.; Dray, A.; Metutera, T.; Metai, E.; Overmars, M. Challenges in freshwater management in low coral atolls. *J. Clean. Prod.* **2007**, *15*, 1522–1528. [[CrossRef](#)]
6. Falkland, A.; Custodio, E.; Diaz Arenas, E.; Simler, E. *Hydrology and Water Resources of Small Islands: A Practical Guide*; UNESCO: Paris, France, 1991; Volume 49, ISBN 9231027530.
7. Terry, J.P.; Thaman, R.R. Physical geography of Majuro and the Marshall Islands. In *The Marshall Islands: Environment, History and Society in the Atolls*; Faculty of Islands and Oceans, the University of the South Pacific: Suva, Fiji, 2008; pp. 1–22.
8. Van der Velde, M.; Javaux, M.; Vanclooster, M.; Clothier, B.E. El Niño–Southern Oscillation determines the salinity of the freshwater lens under a coral atoll in the Pacific Ocean. *Geophys. Res. Lett.* **2006**, *33*, L21403. [[CrossRef](#)]
9. Parry, M.L.; Canziani, O.F.; Palutikof, J.P.; van der Linden, P.J.; Hanson, C.E. Small islands. Climate Change. Climate Change 2007: Impacts, Adaptation and Vulnerability. Contribution of Working Group II to the Fourth Assessment Report of the Intergovernmental Panel on Climate Change. In *Climate Change 2007: Impacts, Adaptation and Vulnerability*; Cambridge University Press: Cambridge, UK, 2007; pp. 671–687.
10. Barkey, B.; Bailey, R. Estimating the Impact of Drought on Groundwater Resources of the Marshall Islands. *Water* **2017**, *9*, 41. [[CrossRef](#)]
11. Terry, J.P.; Falkland, A.C. Responses of atoll freshwater lenses to storm-surge overwash in the Northern Cook Islands. *Hydrogeol. J.* **2010**, *18*, 749–759. [[CrossRef](#)]
12. Fletcher, B.C.H.; Richmond, B.M. *Report of Findings—Climate Change in the Federated States of Micronesia: Food and Water Security, Climate Risk Management, and Adaptive Strategies*; University of Hawai'i Sea Grant College Program: Honolulu, HI, USA, 2010; pp. 1–32.
13. Gingerich, S.B.; Voss, C.I.; Johnson, A.G. Seawater-flooding events and impact on freshwater lenses of low-lying islands: Controlling factors, basic management and mitigation. *J. Hydrol.* **2017**, *551*, 676–688. [[CrossRef](#)]
14. Gingerich, S.B. Groundwater resources and contamination at RoiNamur Island, Kwajalein Atoll, Republic of the Marshall Islands, 1990–91. *Water-Resour. Investig. Rep.* **1996**, *95*, 1–10.
15. Hunt, C.D. Ground-Water Resources and Contamination at Kwajalein Island, Republic of the Marshall Islands, 1990–91. *Water Resour. Investig. Rep.* **1996**, *94*, 1–10.
16. Hejazian, M.; Gurdak, J.J.; Swarzenski, P.; Odigie, K.O.; Storlazzi, C.D. Land-use change and managed aquifer recharge effects on the hydrogeochemistry of two contrasting atoll island aquifers, Roi-Namur Island, Republic of the Marshall Islands. *Appl. Geochem.* **2017**, *80*, 58–71. [[CrossRef](#)]
17. Peterson, F.L.; Gingerich, S.B. Modeling atoll groundwater systems. In *Groundwater Models for Resources Analysis and Management*; El-Kadi, A.I., Ed.; CRC Press: Boca Raton, FL, USA, 1995; pp. 275–292.
18. Terry, J.P.; Chui, T.F.M.; Falkland, A. Atoll Groundwater Resources at Risk: Combining Field Observations and Model Simulations of Saline Intrusion Following Storm-Generated Sea Flooding. In *Groundwater in the Coastal Zones of Asia-Pacific*; Wetzelhuetter, C., Ed.; Springer: Dordrecht, The Netherlands, 2013; pp. 247–270. ISBN 978-94-007-5648-9.
19. Merrifield, M.A.; Merrifield, S.T.; Mitchum, G.T. An anomalous recent acceleration of global sea level rise. *J. Clim.* **2009**, *22*, 5772–5781. [[CrossRef](#)]
20. Vermeer, M.; Rahmstorf, S. Global sea level linked to global temperature. *Proc. Natl. Acad. Sci. USA* **2009**, *106*, 21527–21532. [[CrossRef](#)] [[PubMed](#)]
21. Merrifield, M.A. A shift in western tropical Pacific sea level trends during the 1990s. *J. Clim.* **2011**, *24*, 4126–4138. [[CrossRef](#)]
22. Buddemeier, R.W.; Smith, S.V. Coral reef growth in an era of rapidly rising sea level: Predictions and suggestions for long-term research. *Coral Reefs* **1988**, *7*, 51–56. [[CrossRef](#)]
23. Montaggioni, L.F. History of Indo-Pacific coral reef systems since the last glaciation: Development patterns and controlling factors. *Earth-Sci. Rev.* **2005**, *71*, 1–75. [[CrossRef](#)]
24. Grinsted, A.; Moore, J.C.; Jevrejeva, S. Reconstructing sea level from paleo and projected temperatures 200 to 2100 ad. *Clim. Dyn.* **2010**, *34*, 461–472. [[CrossRef](#)]
25. Nicholls, R.J.; Cazenave, A. Sea-Level Rise and Its Impact on Coastal Zones. *Science* **2010**, *328*, 1517–1520. [[CrossRef](#)] [[PubMed](#)]

26. Storlazzi, C.D.; Shope, J.B.; Erikson, L.H.; Hegermiller, C.A.; Barnard, P.L. Future wave and wind projections for U.S. and U.S.-affiliated pacific islands. *U.S. Geol. Surv. Open-File Rep.* **2015**, *1001*, 1–426.
27. Quataert, E.; Storlazzi, C.; Van Rooijen, A.; Cheriton, O.; Van Dongeren, A. The influence of coral reefs and climate change on wave-driven flooding of tropical coastlines. *Geophys. Res. Lett.* **2015**, *42*, 6407–6415. [[CrossRef](#)]
28. Albert, S.; Leon, J.X.; Grinham, A.R.; Church, J.A.; Gibbes, B.R.; Woodroffe, C.D. Interactions between sea-level rise and wave exposure on reef island dynamics in the Solomon Islands. *Environ. Res. Lett.* **2016**, *11*, 54011. [[CrossRef](#)]
29. U.S. Geological Survey. *National Field Manual for the Collection of Water-Quality Data*; U.S. Geological Survey: Reston, VA, USA, 1998; Book 9, Chapters A1–A9.
30. Swarzenski, P.W.; Simonds, F.W.; Paulson, A.J.; Kruse, S.; Reich, C. Geochemical and Geophysical Examination of Submarine Groundwater Discharge and Associated Nutrient Loading Estimates into Lynch Cove, Hood Canal, WA. *Environ. Sci. Technol.* **2007**, *41*, 7022–7029. [[CrossRef](#)] [[PubMed](#)]
31. Swarzenski, P.W.; Burnett, W.C.; Greenwood, W.J.; Herut, B.; Peterson, R.; Dimova, N.; Shalem, Y.; Yechieli, Y.; Weinstein, Y. Combined time-series resistivity and geochemical tracer techniques to examine submarine groundwater discharge at Dor Beach, Israel. *Geophys. Res. Lett.* **2006**, *33*, L24405. [[CrossRef](#)]
32. Swarzenski, P.W.; Kruse, S.; Reich, C.; Swarzenski, W.V. Multi-channel resistivity investigations of the freshwater-saltwater interface: A new tool to study an old problem. In Proceedings of the International Symposium: A New Focus on Groundwater—Seawater Interactions, Perugia, Italy, 2–13 July 2007; pp. 1–7.
33. Manheim, F.T.; Krantz, D.E.; Bratton, J.F. Studying Ground Water Under Delmarva Coastal Bays Using Electrical Resistivity. *Ground Water* **2004**, *42*, 1052–1068. [[CrossRef](#)]
34. Zektser, I.S.; Dzyuba, A.V. Submarine discharge into the Barents and White Seas. *Environ. Earth Sci.* **2014**, *71*, 723–729. [[CrossRef](#)]
35. Swarzenski, P.W. U/Th Series Radionuclides as Coastal Groundwater Tracers. *Chem. Rev.* **2007**, *107*, 663–674. [[CrossRef](#)] [[PubMed](#)]
36. Burnett, W.C.; Dulaiova, H. Estimating the dynamics of groundwater input into the coastal zone via continuous radon-222 measurements. *J. Environ. Radioact.* **2003**, *69*, 21–35. [[CrossRef](#)]
37. Burnett, W.C.; Bokuniewicz, H.; Huettel, M.; Moore, W.; Taniguchi, M. Groundwater and pore water inputs to the coastal zone. *Biogeochemistry* **2003**, *66*, 3–33. [[CrossRef](#)]
38. Burnett, W.C.; Aggarwal, P.K.; Aureli, A.; Bokuniewicz, H.; Cable, J.E.; Charette, M.A.; Kontar, E.; Krupa, S.; Kulkarni, K.M.; Loveless, A.; et al. Quantifying submarine groundwater discharge in the coastal zone via multiple methods. *Sci. Total Environ.* **2006**, *367*, 498–543. [[CrossRef](#)] [[PubMed](#)]
39. Dulaiova, H.; Burnett, W.C.; Chanton, J.P.; Moore, W.S.; Bokuniewicz, H.J.; Charette, M.A.; Sholkovitz, E. Assessment of groundwater discharges into West Neck Bay, New York, via natural tracers. *Cont. Shelf Res.* **2006**, *26*, 1971–1983. [[CrossRef](#)]
40. Schubert, M.; Paschke, A.; Lieberman, E.; Burnett, W.C. Air–Water Partitioning of ²²²Rn and its Dependence on Water Temperature and Salinity. *Environ. Sci. Technol.* **2012**, *46*, 3905–3911. [[CrossRef](#)] [[PubMed](#)]
41. Swarzenski, P.W.; Dulaiova, H.; Dailer, M.L.; Glenn, C.R.; Smith, C.G.; Storlazzi, C.D. *A Geochemical and Geophysical Assessment of Coastal Groundwater Discharge at Select Sites in Maui and O’ahu, Hawai’i*; Springer: Amsterdam, The Netherlands, 2015; Volume 7, pp. 27–46. ISBN 9789400756472.
42. Gingerich, S.B. Numerical Simulation of the Freshwater Lens on Roi-Namur Island, Kwajalein Atoll, Republic of the Marshall Islands. Master’s Thesis, University of Hawaii, Honolulu, HI, USA, 1992.
43. Greskowiak, J. Tide-induced salt-fingering flow during submarine groundwater discharge. *Geophys. Res. Lett.* **2014**, *41*, 6413–6419. [[CrossRef](#)]
44. Kooi, H.; Groen, J.; Leijnse, A. Modes of seawater intrusion during transgressions. *Water Resour. Res.* **2000**, *36*, 3581–3589. [[CrossRef](#)]
45. Peterson, F.L. Hydrogeology of the Marshall Islands. In *Geology and Hydrogeology of Carbonate Islands. Developments in Sedimentology*; Elsevier: Amsterdam, The Netherlands, 1997; Volume 54, pp. 611–636. ISBN 9781627034470.
46. NASA and RTS Precipitation Measurement Mission Ground Validation. Available online: https://trmm-fc.gsfc.nasa.gov/trmm_gv/data/data.html (accessed on 26 August 2017).

47. Australian Bureau of Meteorology (ABM); Commonwealth Scientific and Industrial Research Organisation (CSIRO). *Climate Variability, Extremes and Change in the Western Tropical Pacific: New Science and Updated Country Reports 2014*; Centre for Australian Weather and Climate Research: Melbourne, Australia, 2014.
48. Cheriton, O.M.; Storlazzi, C.D.; Rosenberger, K.J. Observations of wave transformation over a fringing coral reef and the importance of low-frequency waves and offshore water levels to runup, overwash, and coastal flooding. *J. Geophys. Res. Oceans* **2016**, *121*, 3121–3140. [[CrossRef](#)]
49. Dolan, C.J.; Lyon, A.J. Calculation of Goodwill: Humanitarianism, Strategic Interests, and the U.S. Response to Typhoon Yolanda. *Glob. Secur. Intell. Stud.* **2016**, *2*. [[CrossRef](#)]
50. Chowdhury, M.R.; Chu, P.-S.; Schroeder, T. ENSO and seasonal sea-level variability—A diagnostic discussion for the U.S.-Affiliated Pacific Islands. *Theor. Appl. Climatol.* **2007**, *88*, 213–224. [[CrossRef](#)]
51. Becker, M.; Meyssignac, B.; Letetrel, C.; Llovel, W.; Cazenave, A.; Delcroix, T. Sea level variations at tropical Pacific islands since 1950. *Glob. Planet. Chang.* **2012**, *80–81*, 85–98. [[CrossRef](#)]
52. NOAA (National Oceanic and Atmospheric Administration). Mean Sea Level Trend Kwajalein, Pacific Ocean. Available online: https://tidesandcurrents.noaa.gov/sltrends/sltrends_station.shtml?stnid=1820000 (accessed on 26 August 2017).
53. Levanon, E.; Yechieli, Y.; Gvirtzman, H.; Shalev, E. Tide-induced fluctuations of salinity and groundwater level in unconfined aquifers—Field measurements and numerical model. *J. Hydrol.* **2016**, *551*, 665–675. [[CrossRef](#)]
54. Prieto, C.; Destouni, G. Quantifying hydrological and tidal influences on groundwater discharges into coastal waters. *Water Resour. Res.* **2005**, *41*, 1–12. [[CrossRef](#)]
55. Moosdorf, N.; Stieglitz, T.; Waska, H.; Dürr, H.H.; Hartmann, J. Submarine groundwater discharge from tropical islands: A review. *Grundwasser* **2014**, *20*, 53–67. [[CrossRef](#)]
56. Tait, D.R.; Santos, I.R.; Erler, D.V.; Befus, K.M.; Cardenas, M.B.; Eyre, B.D. Estimating submarine groundwater discharge in a South Pacific coral reef lagoon using different radioisotope and geophysical approaches. *Mar. Chem.* **2013**, *156*, 49–60. [[CrossRef](#)]
57. Santos, I.R.; Erler, D.; Tait, D.; Eyre, B.D. Breathing of a coral cay: Tracing tidally driven seawater recirculation in permeable coral reef sediments. *J. Geophys. Res. Oceans* **2010**, *115*, 1–10. [[CrossRef](#)]
58. Knee, K.L.; Crook, E.D.; Hench, J.L.; Leichter, J.J.; Paytan, A. Assessment of Submarine Groundwater Discharge (SGD) as a Source of Dissolved Radium and Nutrients to Moorea (French Polynesia) Coastal Waters. *Estuaries Coasts* **2016**, *39*, 1651–1668. [[CrossRef](#)]
59. Cardenas, M.B.; Zamora, P.B.; Siringan, F.P.; Lopus, M.R.; Rodolfo, R.S.; Jacinto, G.S.; San Diego-McGlone, M.L.; Villanoy, C.L.; Cabrera, O.; Senal, M.I. Linking regional sources and pathways for submarine groundwater discharge at a reef by electrical resistivity tomography, ²²²Rn, and salinity measurements. *Geophys. Res. Lett.* **2010**, *37*. [[CrossRef](#)]
60. Taniguchi, M.; Burnett, W.C.; Cable, J.E.; Turner, J.V. Investigation of submarine groundwater discharge. *Hydrol. Process.* **2002**, *16*, 2115–2129. [[CrossRef](#)]
61. Korom, S.F. Natural denitrification in the saturated zone: A review. *Water Resour. Res.* **1992**, *28*, 1657–1668. [[CrossRef](#)]
62. Burt, R.A. Ground-water chemical evolution and diagenetic processes in the upper Floridan Aquifer, southern South Carolina and northeastern Georgia. *USGS Water Supply Pap.* **1993**, *2392*, 1–76.
63. Presley, T.K. *Majuro Water and Sewer Company, Majuro Atoll, Republic of the Marshall Islands Effects of the 1998 Drought on the Freshwater Lens in the Laura Area, Majuro Atoll, Republic of the Marshall Islands*; Scientific Investigations Report 2005-5098; Geological Survey (U.S.): Reston, VA, USA, 2005; 40p.
64. Storlazzi, C.D. SERDP Project RC-2334: The Impact of Sea-Level Rise and Climate Change on Department of Defense Installations on Atolls in the Pacific Ocean. Available online: <https://www.serdp-estcp.org/Program-Areas/Resource-Conservation-and-Resiliency/Infrastructure-Resiliency/Vulnerability-and-Impact-Assessment/RC-2334/RC-2334> (accessed on 26 August 2017).
65. Australian Bureau of Meteorology (ABM); Commonwealth Scientific and Industrial Research Organisation (CSIRO). *Current and Future Climate of the Marshall Islands*; CSIRO, Australian Bureau of Meteorology: Melbourne, Australia, 2015; pp. 1–11.
66. Reynolds, M.H.; Courtot, K.N.; Berkowitz, P.; Storlazzi, C.D.; Moore, J.; Flint, E. Will the effects of sea-level rise create ecological traps for Pacific island seabirds? *PLoS ONE* **2015**, *10*, e0136773. [[CrossRef](#)] [[PubMed](#)]

67. PacIOOS Wave Run-Up Forecast: Kwajalein, RMI. Available online: <http://www.pacioos.hawaii.edu/shoreline/runup-kwajalein/> (accessed on 26 August 2017).
68. Van Vuuren, D.P.; Edmonds, J.; Kainuma, M.; Riahi, K.; Thomson, A.; Hibbard, K.; Hurtt, G.C.; Kram, T.; Krey, V.; Lamarque, J.F.; et al. The representative concentration pathways: An overview. *Clim. Chang.* **2011**, *109*, 5–31. [[CrossRef](#)]
69. Science, P.C.C.; Program, A.P. *Pacific-Australia Climate Change Science and Adaptation Planning Program Climate Variability, Extremes and Change in the Western Tropical Pacific: New Science and Updated Country Reports*; Australian Bureau of Meteorology and Commonwealth Scientific and Industrial Research Organisation (CSIRO): Canberra, Australia, 2014; ISBN 9781486302888.



© 2017 by the authors. Licensee MDPI, Basel, Switzerland. This article is an open access article distributed under the terms and conditions of the Creative Commons Attribution (CC BY) license (<http://creativecommons.org/licenses/by/4.0/>).